ISSN 0016-8521, Geotectonics, 2018, Vol. 52, No. 4, pp. 401–420. © Pleiades Publishing, Inc., 2018.
Original Russian Text © S.Yu. Sokolov, A.O. Mazarovich, N.N. Turko, K.O. Dobrolyubova, A.S. Abramova, Yu.A. Zaraiskaya, E.A. Moroz, 2018, published in Geotektonika, 2018, No. 4, pp. 3–24.

Deformations and Manifestations of Degassing in the Sedimentary Cover of the Equatorial Segment of the West Atlantic: Implications for Lithospheric Geodynamics

S. Yu. Sokolov[a, *], A. O. Mazarovich[a], N. N. Turko[a], K. O. Dobrolyubova[a], A. S. Abramova[a], Yu. A. Zaraiskaya[a], and E. A. Moroz[a]

[a]*Geological Institute, Russian Academy of Sciences, Moscow, 119017 Russia*

**e-mail: sysokolov@yandex.ru*

Received November 25, 2017

Abstract—Manifestations of fluids and deformations in the sedimentary cover, which are both factors of brightening (blanking anomalies) in seismoacoustic records, in the equatorial segment of the Atlantic coincide with the sublatitudinal zones of the activated passive parts of transform faults and with zones of lower gravity anomalies and higher values of remnant magnetization, which form as a result of serpentinization. The cause-and-effect sequence of intraplate phenomena includes: the contrasting geodynamic state → horizontal movements that form macrofractures → water supply to the upper mantle → serpentinization of rocks in the upper mantle → deformations associated with vertical uplift of basement and sedimentary cover blocks, coupled with fluid generation → and fluid accumulation in the sedimentary cover, accompanied by the formation of anomalies in seismoacoustic records. Based on the seismic data, we have identified imbricate-thrust deformations, diapir structures, stamp folds, and positive and negative flower structures, indicating the presence of strike-slip faults in the passive parts of transform faults. The general spatial distribution of deformation structures shows their concentration in cold mantle zones. Correlative comparison of the structural characteristics of deformations shows the direct relationship between the heights of structures and the development of serpentinization processes. As per the age of the basement, deformations range from 27–38 to 43–53 Ma; a quite thick sedimentary cover makes it possible to reveal them based on the characteristic types of seismoacoustic records. The formation of the Antilles arc ca. 10 Ma ago affected the equatorial segment of the Atlantic; it formed kink bands where lithospheric blocks underwent displacements with counterclockwise rotations, deformations related to compression and vertical uplift of crustal fragments, and local extension that favored degassing of endogenous fluids. Sublatitudinally oriented imbricate-thrust deformations with different vergences indicate irregularity and alternating strike-slip directions as blocks between fractures were laterally influenced.

Keywords: equatorial Atlantic, cold mantle blocks, geodynamics, serpentinization, deformations of the sedimentary cover, degassing, passive parts of transform faults

DOI: 10.1134/S0016852118040076

INTRODUCTION

Deformations of the sedimentary cover in the deep-water part of the Atlantic have been repeatedly described in the literature (for example, see [1, 3, 5, 7, 9, 11–13, 17] and others). These works were based on the data obtained during the expeditions conducted in the period since 1984 until 2006. They included the studies within two large regions: (a) along the Angola–Brazil geotraverse carried out by the Institute of Oceanology, Academy of Sciences of the USSR, in the period from 1984 to 1986 under the Ministry of Geology and Academy of Sciences of the USSR, (b) and in the equatorial segment of the Atlantic (ESA) carried out by the Geological Institute of the Russian Academy of Sciences (hereinafter, GIN RAS) aboard the R/V *Akademik Nikolai Strakhov.* In the foreign literature, there is the publication summarizing the copious data on continental margins and the deep-water part of the Atlantic [21]. It was determined in this work that the postrift sedimentary supersequence, which occurs on the rift supersequence of the margins and igneous basement of the ocean, is a sedimentary structure generally undisturbed by other tectonic deformations, with layers dipping gently towards the spreading center and wedging at the acoustic basement. In the opinion of the authors of [21], the only exceptions are active consedimentation normal faults, plastic salt flows, faults caused by movement of salt and subsidence of the covering sequence, faults in the rift supersequence of the perioceanic zone with disturbed isostatic equilibrium, as well as mud volcanism and igneous intru-

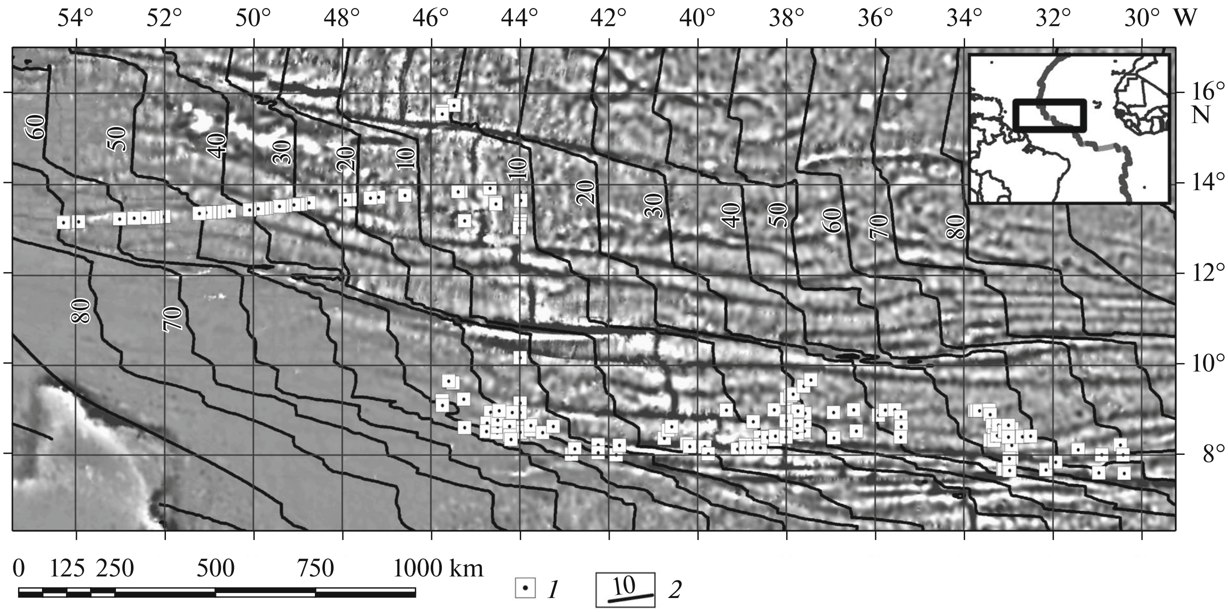

Fig. 1. Distribution of structures undifferentiated by type related to vertical uplift of basement and sedimentary cover, based on data from cruises 6 and 9 of the R/V *Akademik Nikolai Strakhov* (GIN RAS, 1987, 1990), and their comparison to basement age and residual relief on topographic basis. Inset: location of study region in Atlantic with respect to MAR: (*1*) structures related to vertical uplift, (*2*) isolines and values of basement age, Ma.

sive bodies. This conclusion was responsible for the corresponding approach to studying deformations in the Atlantic. However, further study of the sedimentary cover in oceanic basins showed the tectogenic factors that form intraplate deformations in the deep-water part of the ocean.

This study is based on the results obtained by GIN RAS in the ESA. Among the deformation structures in abyssal parts of the ESA, the predominant contribution comes from those related to vertical uplift of the sedimentary cover by narrow blocks in the basement (diapir, or piercement, structures) of both recent and present-day ages (in terms of the extent of deformation in the section), by wide blocks in the basement (stamp folds), degassing-related uplift, and transpressive stress. In [7], based on continuous seismic profiling (CSP) data obtained during cruises 6 and 9 of the R/V *Akademik Nikolai Strakhov* (GIN RAS, 1987 and 1990; both cruises led by Yu.N. Raznitsin; the head of the CSP party was V.M. Poberzhin) in areas of such fracture zones as the Marathon, Mercury, Arkhangelsky, Doldrums, and Vernadsky; primary analysis of the spatial distribution of these structures was conducted, as well as their statistical characteristics without differentiation by deformation type. The general statistical characteristics of structures with vertical uplift were studied. It was found that the main spatial cluster of deformations was related to NW-oriented kink band structures, which cause bends in the branches of transform faults in the northern segment of the ESA (Fig. 1) between 7° and 15° N, on both flanks of the Mid-Atlantic Ridge (MAR). Nevertheless, preliminary analysis of different types of deformations showed that they differ in spatial arrangement with respect to the tectonic elements of the ocean floor; this suggests the need for further study and interpretation of their genesis. The aim of the present work is to define structural references for deformations of various types and degassing zones in the sedimentary cover, and to compare them with macrofractures, gravity, and magnetic fields, their transform faults, as well as with seismotomographic data indicating the geodynamic state of the mantle. The ultimate task is to determine how the origins of deformation structures from detailed CSP data fit the cause-and-effect sequence of intraplate phenomena, which consists of the following steps (after [17], with additions):

(1) the horizontally contrasting geodynamic state of the mantle;

(2) inhomogeneous horizontal movements forming a higher degree of macrofracturing, including tectonic shear deformations, during cooling of the lithosphere;

(3) water supply to the upper mantle through the formed macrofractures;

(4) creation of conditions for serpentinization of upper mantle rocks with the formation of decompaction zones, local negative gravity anomalies, and higher magnetization anomalies;

(5) deformations related to the vertical uplift of blocks of the basement and sedimentary cover and fluid generation (mainly methane);

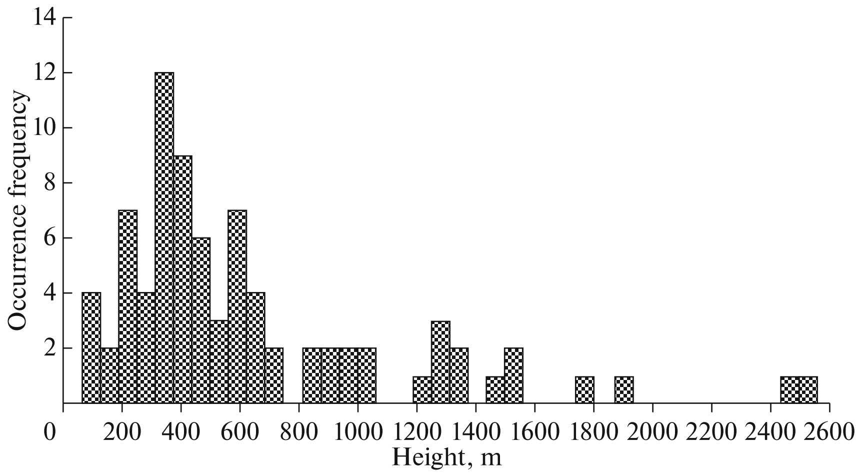

Fig. 2. Occurrence frequency for heights of structures related to vertical uplift, as measured for basement.

(6) accumulation of fluids in the sedimentary cover, formation of anomalies in seismoacoustic records, and penetration of fluids into water.

PRIMARY RESULTS WITHOUT SEPARATION OF STRUCTURES INTO TYPES

The results obtained from the general analysis of the statistical characteristics of deformation structures can be formulated as follows. The histogram for the heights of structures undifferentiated by type (Fig. 2) shows that the most frequently observed are about 400 m. The origination of vertical movements related to serpentinization of upper mantle rocks and a 20% increase in their volume suggest that the thickness of the layer involved in this process is up to 2 km. Given that this process could not have taken place in the entire rock volume, but only along fractures, the real depth of rock alteration may be higher. The height distribution shows weak signs of polymodality, in particular, at 1300 m (Fig. 2). This may indicate both the presence of individual large diapirs and activation of processes in the vicinity of these structures; note that recognition of such activation for each structure requires particular analysis of the seismic wave field.

It is feasible to analyze the properties of deformed objects depending on the age of the substrate on which they formed (Fig. 3). This approach can replace, to certain degree, estimation depending on the distance from the MAR. The values of ages were taken from [25]. We can reliably see a descending pseudolinear dependence of the depth of the bottom near the mentioned structures. Such a trend is not very predictable because, in accordance with the model representation in [18], the trend should look like the descending curve of the square root of age. The real trend is, however, gradual around 20 Ma and up until around 60 Ma has a gentle slope. The heights of structures are arranged as an inclined band with a gentle ascent from 400 to 600 m up until 20 Ma and then with a gentle increase to ~700 m. Three intervals of higher values of the age parameter (6–16, 27–38, and 43–53 Ma, or Middle–Late Miocene, Oligocene, and Early–Middle Miocene, respectively) are superimposed on this band (Fig. 3). These intervals are similar to those when deformations were manifested along the geotraverse on the western flank of the MAR [17], but with a shift of 7–8 Ma toward younger ages with respect to the MAR. As well, the intervals continue to overlap. Given the pseudoperiodic evolution of the magnetic properties of serpentinites depending on temperatures in the upper mantle [14], this distribution can be interpreted as a local activation and continuation of diapiric processes when certain temperatures are reached. Notably, the zone affected by deformations can be repeatedly activated when the medium attains the next temperature interval of serpentinization processes. The age of the substrate does not fit the ages of structures, but it may illustrate the evolution of the temperature state with time. Figure 3 also shows the ages of discontinuities in the bottom relief gradient—20 and 60 Ma—from [15]. These ages fall in the gaps between age zones with anomalous folding of the basement. In [15], these discontinuities were explained by the change in density of the upper mantle due phase transitions during crystallization at the base of the lithosphere: such changes result in a nongradual change in averaged relief according to the root-of-age law. Such a combination indicates a certain sequence of changes in the structure of the lithosphere during its cooling.

TYPES OF DEFORMATION STRUCTURES

There are different approaches to categorizing types of deformation. The deformation structures in the Northwest Pacific, obtained from CSP data, were reviewed in [6]. According to [6], the types of structures include the so called injective and tectonic

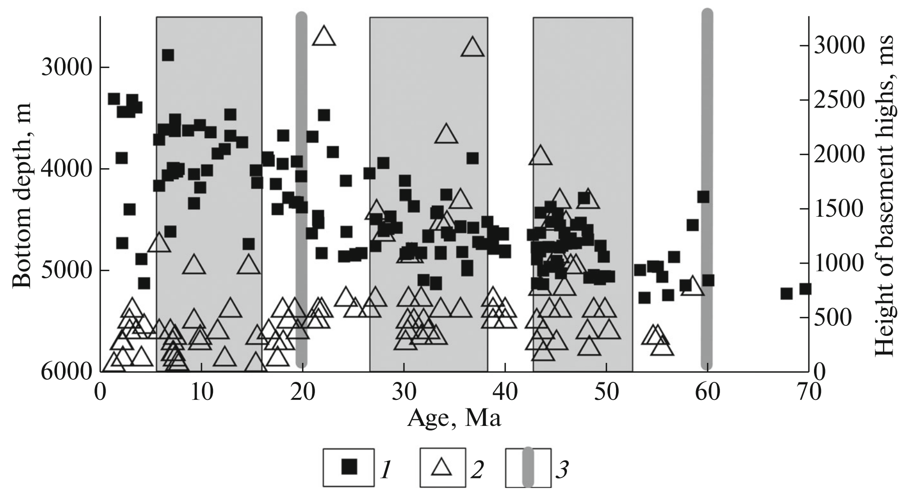

Fig. 3. Distribution of heights of diapir structures and bottom depths above them versus age of igneous substrate. Age intervals with higher values of heights of basement highs are shown in gray columns: (*1*) bottom depths; (*2*) heights; (*3*) ages of break points in bottom relief.

mounds. If to compare these types to the traditional terminology, asymmetric tectonic mounds limited by reverse faults in one side are the manifestations of imbricate-thrust deformations. Injective mounds are diapiric (piercement) structures, or stamp folds at wide basement blocks. In addition, the author of [6] distinguished the complex of deformations related to fluid ascent and anomalies of sediments bedding (the latter related to contour currents and turbidite flows). Deposits of flows are widespread in the abyssal zone, but they are not of tectonic origin there. For example, these are the most common soils in taxonomy of structural anomalies in the abyssal sedimentary cover: they differ from the simplest seismofacies of filling, which is theoretically the main one in basins. However, real observations in the studied basin of the Pacific [6] have shown that there are zones where this seismofacies is not detected. Study [17] presented a list of types of deformations studied in the ESA along the western passive parts of the Marathon and Mercury transform faults; analogously to deformations in the Pacific, they were predominantly represented by (a) structures with vertical uplift or sediments pierced by basement blocks with different widths and (b) structures and seismoacoustic record patterns caused by the fluid factor. Structures with vertically displaced negative reflectors are rare.

The zone with the most intense development of deformation structures in the ESA is the study region of cruise 9 of the R/V *Akademik Nikolai Strakhov*. We used the following technique to process the CSP data. Since the distance between traverses during these works ranged from 5 NM in small areas to 30 NM during reconnaissance traverses to cover areas as large as about 1000 × 500 km, correlation of reflectors with thicknesses of no more than 1000 m and occurring on fragmented igneous basement, in order to construct a continuous surface of reflectors, is problematic. These data allow us, using the picking approach to indicated peculiarities of the wave field in problem-oriented software (RadExPro developed by RadExPro Seismic Software, Russia), to reveal and digitize spatial locations and quantitative characteristics for multiple dislocations of normal and reverse fault types, stamp folds, diapir structures, acoustic blanking anomalies of seismoacoustic records, flat-topped basement uplifts, drifts, and others. These peculiarities of the wave field, along with the vectors of such parameters as width, height, and thickness of sediments above basement folding, form a database that is updated jointly with available spatial coverage and supplemented by geophysical field values, whose interpretation has geodynamic implications. The most widespread (frequently occurring) types of deformations in the sedimentary cover within the study region are: vertical acoustic blanking anomalies in seismoacoustic records, or gas pipes (Fig. 4, profiles 1, 2); stamp folds (Fig. 4, profiles 9, 10); diapir structures (Fig. 4, profiles 8, 9); individual reverse faults (Fig. 4, section 7); imbricate-thrust systems of reverse faults (Fig. 4, profile 3); horizontal acoustic blanking anomalies in seismoacoustic records (Fig. 4, profiles 2, 7); and normal faults (Fig. 4, profile 4).

These mentioned types, with the exception of normal faults, can be combined into groups based on the same principle as in [6]. Erosional-accumulative forms owing to currents contain incuts and drifts (Fig. 4, profile 2), natural levees (Fig. 4, profile 5), and landslides (Fig. 4, profile 11).

Types of deformation not reported earlier for basins should be mentioned in particular: these are positive and negative flower structures (Fig. 4, profiles 5, 6). Negative flower structures form during shear displacement of lithospheric blocks with elements of compres-

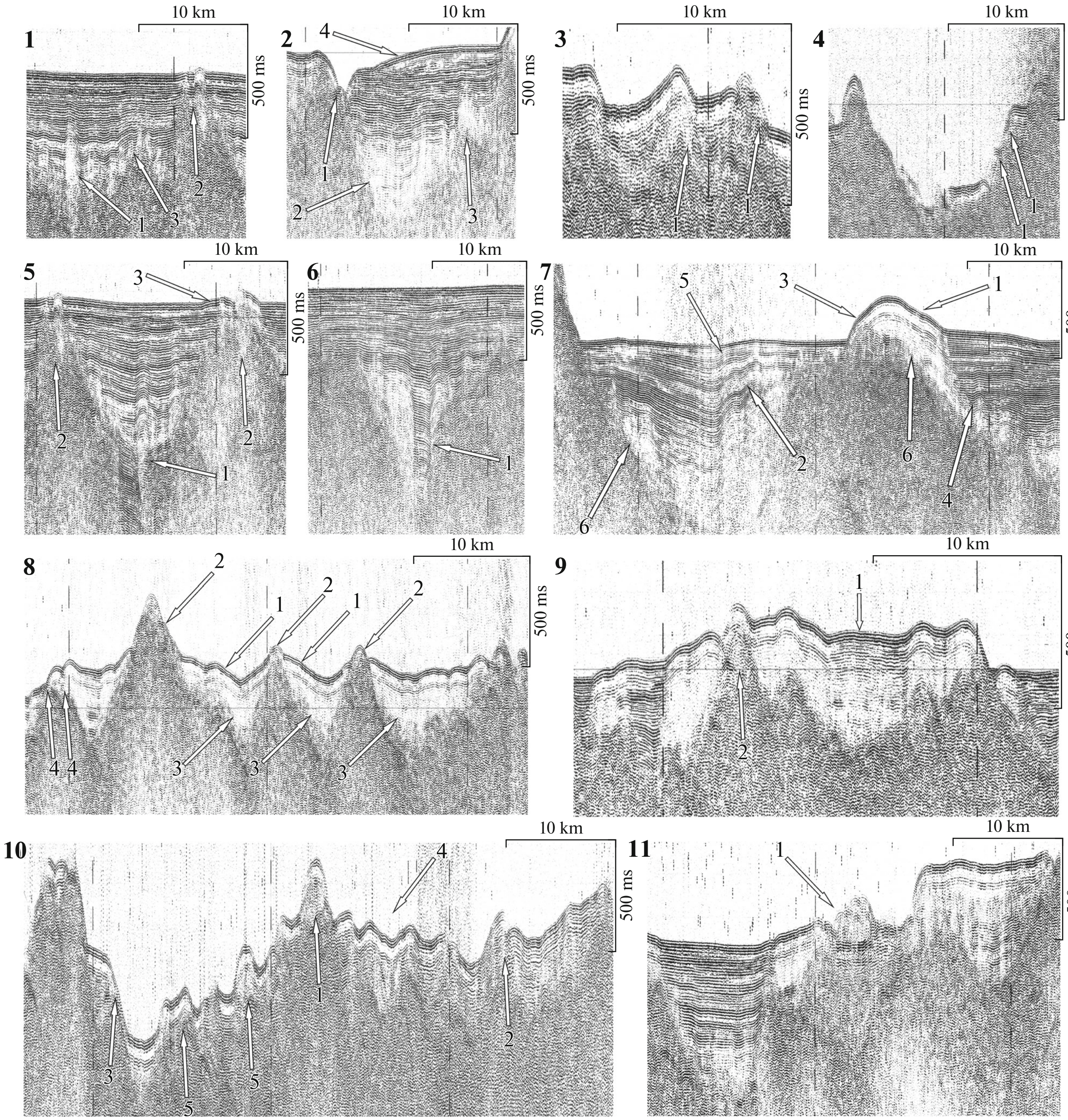

Fig. 4. Main types of deformation structures, based on CSP data from cruise 9 of R/V *Akademik Nikolai Strakhov* (GIN RAS, 1990). Numbered arrows indicate structural features in seismic sections (SS; their numbers are in boldface): **SS 1**: 1, vertical acoustic blanking anomaly in sedimentary cover; 2, diapir structures; 3, plicative folds. **SS 2**: 1, incut; 2, horizontal acoustic blanking anomaly in sedimentary cover; 3, vertical acoustic blanking anomaly in sedimentary cover; 4, drift. **SS 3**: 1, reverse faults and thrusts. **SS 4**: 1, normal faults. **SS 5**: 1, positive flower structures; 2, diapir structures; 3, natural levee. **SS 6**: 1, negative flower structures. **SS 7**: 1, reflectors inclined at >1° in sedimentary cover; 2, constant thickness between reflectors in folded-type record; 3, disjunctive dislocations; 4, diapir structures; 5, structural unconformities; 6, acoustic blanking anomaly in sedimentary cover in form of lenses and gas chimneys. **SS 8**: 1, reflectors inclined at >1° in sedimentary cover; 2, diapir structures; 3, acoustic blanking anomaly in sedimentary cover in form of lenses and gas chimneys; 4, disjunctive dislocations. **SS 9**: 1, broad stamp fold; 2, diapir structures. **SS 10**: 1, diapir structures; 2, reverse faults and thrusts; 3, normal faults; 4, plicative folds; 5, narrow stamp fold. **SS 11**: 1, landslide body.

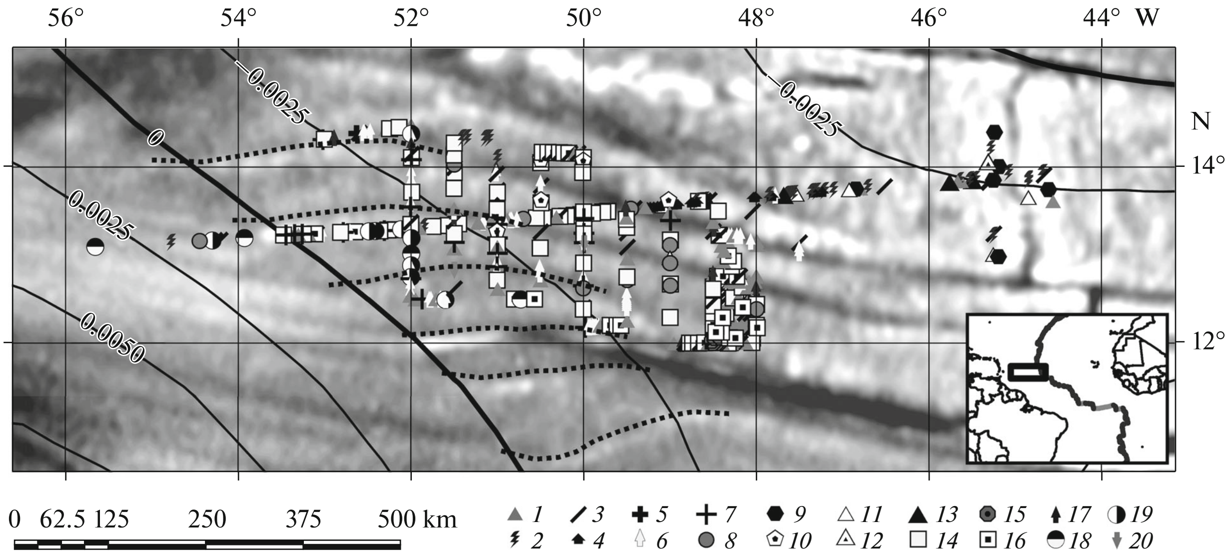

Fig. 5. General spatial distribution of deformations and other anomalous types in seismoacoustic records as obtained when interpreting point-based peculiarities of wave field during cruise 9 of R/V *Akademik Nikolai Strakhov* (GIN RAS, 1990). Inset: location of study region. Topographic basis is satellite altimetry data with data from [26]. Isolines with values are for mobility attribute $\delta(Vp/Vs)$, after [17]; dotted lines denote bends of kink-band structures. Deformations and anomalous types in seismoacoustic record: (*1*) diapir structure; (*2*) normal fault; (*3*) reverse fault; (*4*) hinge; (*5*) paleochannel; (*6*) vertical acoustic blanking anomaly; (*7*) horizontal acoustic blanking anomaly; (*8*) bright spot; (*9*) flat top; (*10*) landslide; (*11*) sediment discharge; (*12*) volcanic edifice; (*13*) basement intrusion; (*14*) stamp fold; (*15*) bending fold; (*16*) imbricate-thrust folds; (*17*) positive flower structure; (*18*) natural levee; (*19*) drift; (*20*) negative flower structure.

sion or extension. Remarkably, these objects were revealed in the passive parts of transform faults, objects for which displacement is theoretically absent. Nevertheless, based on data on the difference between spreading rates in adjacent blocks of oceanic crust (sometimes it differs by a factor of 2–3 [10]) and under the assumption about the geodynamic implications of this [16], we can conclude that shearing in the passive parts of transform faults is theoretically possible. Detection of near-fault flower structures in CSP images within the sediment-filled passive parts of fault troughs indicates the true existence of this process and obviously supports it with facts.

GENERAL SPATIAL DISTRIBUTION OF DEFORMATIONS

The general spatial distribution of deformation-related and other anomalous patterns in seismoacoustic records (Fig. 5) is related to the survey route, but the obtained cluster of points does not mean the absence of any forms in between traverses. Morphological interpolation of the space between traverses is carried out on a topographic basis (satellite altimetry data [26]), which also reflects the structure of the acoustic basement beneath the sedimentary cover. The isolines in Fig. 5 show the values of mobility attribute, after [17]; negative values of this attribute indicate “cold” lenses in the upper mantle at a depth of about 470 km depth. The minimum attribute values reflecting the values of the Poisson coefficient and indicating the geodynamic state correlate with the degree of macrofracturing on the surface [16] and determine the distribution of surface geophysical characteristics. The different rheological properties at the mentioned depth result in (a) more mobile dynamics in “hot” zones with a lower viscosity of mantle material and (b) a higher degree of macrofracturing above cold blocks. Their interaction creates conditions for additional faulting in cold blocks, especially for irregular spreading rates along coeval basement zones [25]. Thus, the first two elements of the sequence of intraplate events—a contrasting geodynamic state of the mantle and macrofracturing—are in a cold zone (Fig. 5).

In the studied segment of the Atlantic (Fig. 5), the following types of deformations appear with the corresponding number: 76 diapir structures, 65 stamp folds, 40 imbricate thrusts, 72 reverse faults, 68 vertical acoustic blanking anomalies, and 22 horizontal acoustic blanking anomalies.

The deformations revealed from the structure of the sedimentary cover [17] are predominantly concentrated above the cold mantle zone to the east of the zero isoline of $\delta(Vp/Vs)$ attribute. Additionally, this isoline is also the western boundary of kink bands (Fig. 5) manifested in the acoustic basement structure. Deformation structures revealed from the detailed CSP data along traverses are very compactly arranged

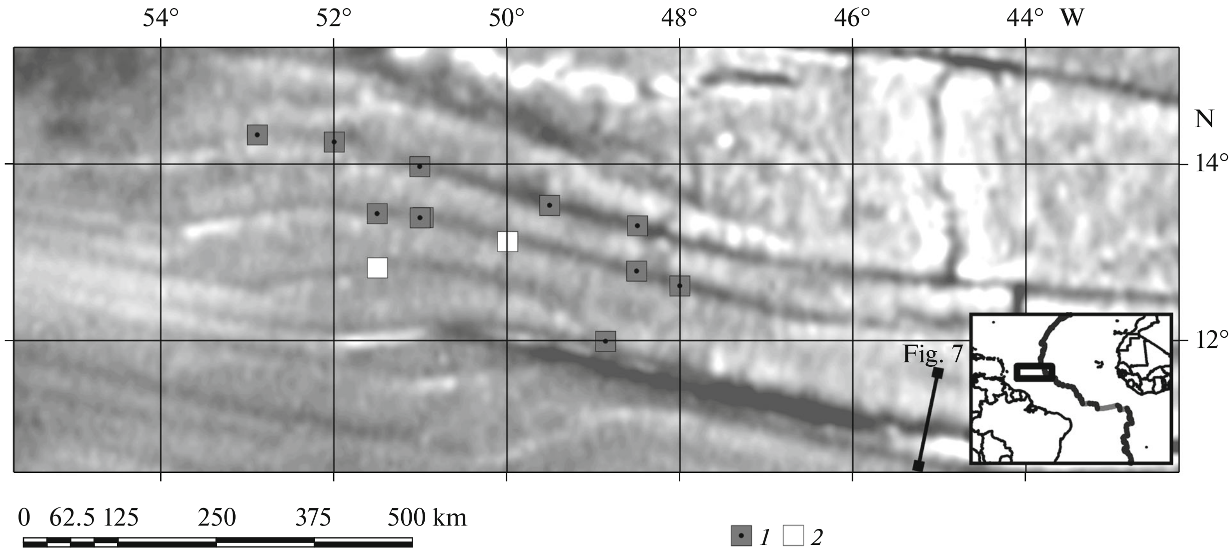

Fig. 6. Spatial distribution of flower-type deformations in sedimentary cover of fault troughs, based on data from cruise 9 of R/V *Akademik Nikolai Strakhov* (GIN RAS, 1990). Inset: location of study region. Topographic basis is satellite altimetry data with data from [26]. Named line shows location of section in corresponding figure. Types of flower structures: (*1*) positive; (*2*) negative.

within the boundaries of the cold segment revealed from processing of fine-scale seismic tomography and altimetry data. The agreement of these results also verifies the relationship between the state of mantle and distribution of deformation structures. The density of deformation structures, especially folds, noticeably decreasing nearing the MAR because of (a) the small thickness of sediments from whose structure these deformations were revealed and (b) manifestations of sediments in the forms of small isolated pockets in depressions in the acoustic basement. In the present study, intermediate elements of the sequence of intraplate phenomena, related to alteration of material, are not considered. The presented data concern only the implications of their processes: they are expressed as deformations and manifestations of fluid supply to the sedimentary cover.

DISTRIBUTION OF STRIKE-SLIP DEFORMATIONS

Strike-slip deformations form a paragenesis that includes the compression structures along the fault. In seismic sections of the sedimentary cover, which are orthogonal to the shear plane, shear deformations are seen as specifically shaped flower structures, one of which is shown in profile 5 of Fig. 4. Arrow 1 in the middle part of the fault trough marks an antiform with no basement folding at its base; this antiform is characterized by an attenuating amplitude for the shift of reflectors upsection and by contrasting reflectors from the sides of the fault trough on both sides of the fault. Such a wave field is formed under transpressive conditions as a positive flower structure. Transtension forms negative flower structures characterized by sinking of reflectors (Fig. 4, section 6). The presence of such structures in the sedimentary cover of the passive parts of transform faults indicates shear displacements between segments of oceanic lithosphere after their movement beyond the active parts of faults as a result of spreading. This phenomenon is theoretically possible [16] owing to the difference in spreading rates of segments along the MAR, as much as 2.5-fold. Since this difference leads to additional displacement beyond the limits of the active parts of transform faults, the sedimentary cover accumulated in passive parts can experience shear deformations. In addition, the formed fracture zone is a zone of weakness and can contain serpentinites, which favor displacements when faults are reactivated.

Figure 6 shows the spatial distribution of the revealed shear deformations (flower structures) in the sedimentary cover of faults to the west of the MAR. Positive flower structures are located chiefly at the bend of the Marathon and Mercury faults, which frame the kink-band-like structural zone in the north, indicating a transpressive regime that formed such a structural pattern of fault troughs. Within this framing, we revealed the more rarely occurring negative flower structures which suggested the presence of an extensional component. The spatial density of these structures was determined by a discrete network of surveying traverses. In fact these deformations may be represented by elongated structures. Thus, origination of this deformation zone was characterized by mosaicity in the stress distribution, with the formation of extension in the internal part.

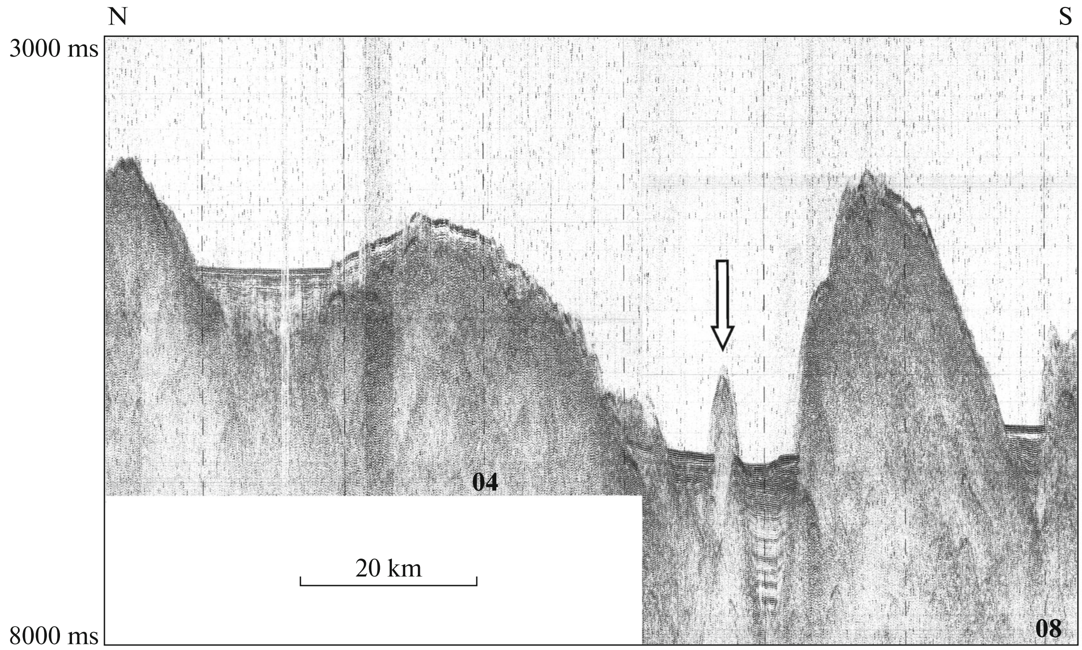

Fig. 7. Fragment of CSP profile no. S09-04 across western passive part of Vema Fracture Zone, based on data from cruise 9 of R/V *Akademik Nikolai Strakhov* (GIN RAS, 1990). Arrow indicates location of median ridge in fault trough.

The studied segment is framed in the south by the western passive part of the Vema Fracture Zone, where a median ridge is observed in the altimetry field, indicating shear with compression. During expeditionary works, this structure was traversed only by the survey transect along ~45° W (Fig. 7), which is 300 km east of the revealed flower structures. We can see the median ridge in the shown section: it rises 450 m above the bottom; it has a total height of about 1350 m and a width of about 1200 m on the bottom; it intruded into sediments to form small-amplitude plicative folding on the reflector at a depth of about 200 ms (Fig. 7). Thus, the median ridge is of variable height along its western continuation and approaches the northern side of the Vema Fracture Zone (Fig. 7), on which there are deformations related to the movements of wide (more than 20 km) basement blocks. Transpressive conditions are observed in the majority of the passive parts of faults framing the zone of kink bands, which can be quite reliably inferred from the distribution of the mapped deformations in the sedimentary cover. The seismoacoustic section to the south of the median ridge (Fig. 7) indicates the presence of intensive bottom currents that formed erosional-accumulative objects.

CORRELATION BETWEEN DEFORMATIONS AND GEOPHYSICAL FIELDS

Comparison between deformations, for which we digitized such quantitative characteristics as width, height, and thickness of sediments above folding of the basement, on the one hand, and geophysical fields, for which structural and geodynamic interpretations are available, on the other, makes it possible to obtain approximate models of their mutual dependences through correlations between numerical values of the mentioned characteristics and values of fields and ages. The models can be expressed quite easily by clusters of points or have a dispersed character, barely showing a trend. For correlations, we used Bouguer anomalies calculated from altimetry data [26] and bottom relief; magnetization used in correlation was calculated from anomalous magnetic field (AMF) [24] and bottom relief data for a magnetized layer 500 m thick, from bottom relief data only [27], and from ages according to the linear magnetic anomalies [25]. Bouguer anomalies mainly reflect the relief of the crustal—mantle interface, and the less the value of this anomaly the deeper this interface occurs. These anomalies also reflect density inhomogeneities in the crust and upper mantle, which are especially contrasting in the MAR zone due to thermal anomalies and nonuniform magmatism. Density inhomogeneities also include serpentinization-related decompaction zones. Magnetization is mainly represented by two components: thermo-remnant, which decreases with distance from the MAR, and chemo-remnant, which forms during serpentinization and conceals magnetization. Thus, the mentioned parameters reflect the processes of fracturing and accretion of an inhomogeneous structure of the igneous spreading basement. The relief is the top of the crustal layer and an indicator of inhomogeneities related to deformations in the sedimen-

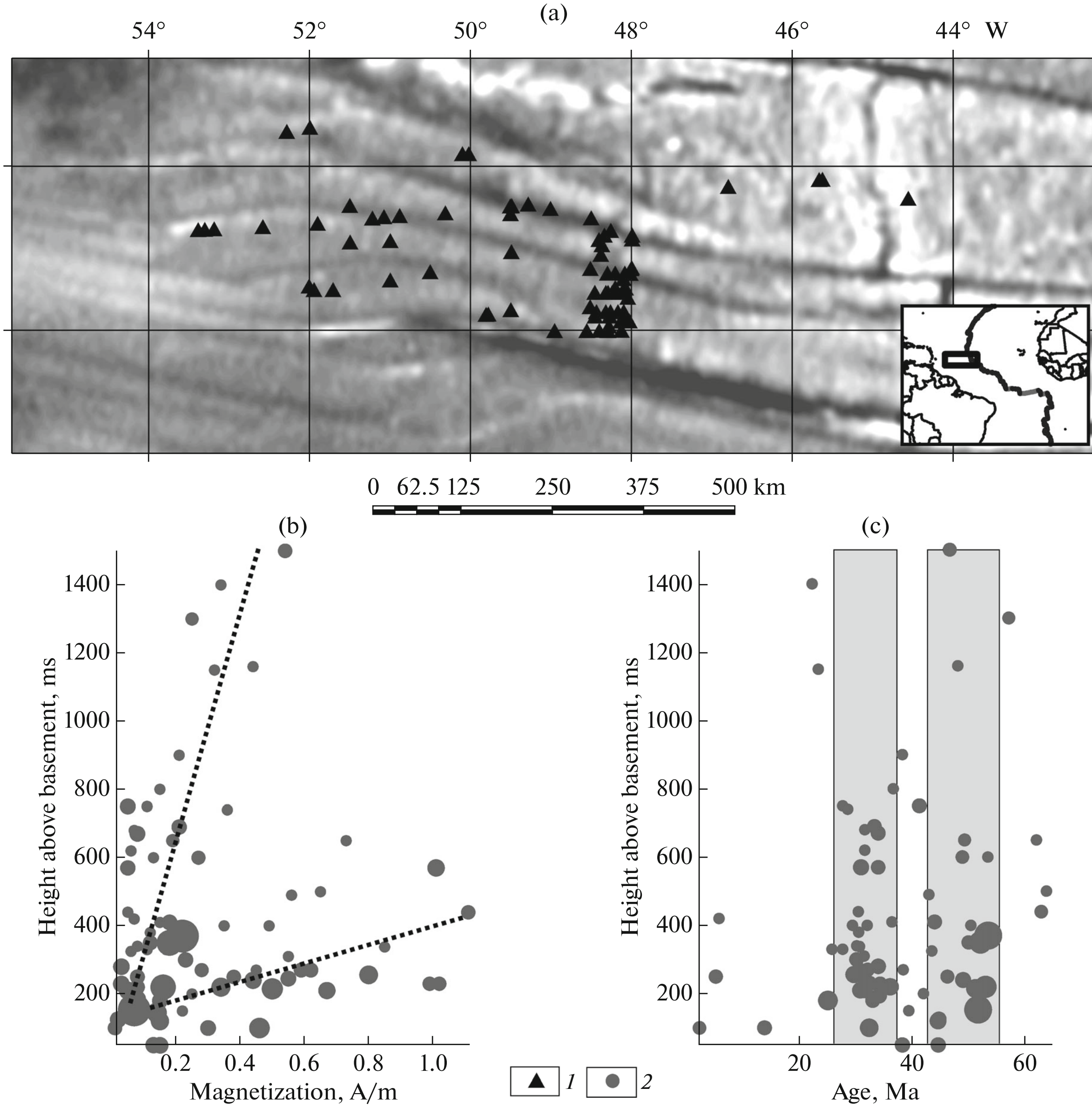

Fig. 8. Diapir structures in ESA west of MAR, based on data from cruise 9 of R/V *Akademik Nikolai Strakhov* (GIN RAS, 1990). (a) General spatial distribution of diapir structures (inset: location of study region); (b) correlation between magnetization calculated from data on anomalous magnetic field and relief combined with heights of diapir structures above basement (dashed lines denote trends and sizes of filled circles proportional to thickness of sediments above tops of structures, from 0 to 520 m); (c) correlation between heights of diapir structures above basement and basement age (intervals of basement ages with higher density of diapir structures are marked by gray columns): (*1*) locations of diapir structures (in panel (a)); (*2*) diapir structures in correlation coordinates (in panels (b) and (c)).

tary cover. The age of the basement is the key parameter forming the evolutionary relationship between structures; it indirectly reflects their thermal history.

CORRELATION BETWEEN THE MAIN TYPES OF DEFORMATIONS

Diapir Structures

An overview of diapir structures (Fig. 4, sections 1, 5, 7, 8) shows that they are ubiquitous along the surveyed traverses (Fig. 8), but tend predominantly toward blocks between fractures and not fault troughs as do flower structures. A dense cluster of these objects in the interval of 48°30′–48°00′ W is related to the survey area. To the west of this area, the distance between traverses is 30 arc min and the zone between 48°30′ and 50°30′ W within its limits is characterized by minimum density of diapir structures (Fig. 8a). In general, this zone fits the zone of local extension revealed by negative flower structures (Fig. 6), but an exact out-line of its boundaries is hardly possible, because it is revealed by a regional survey network. The fit of local extension zones and zones with a low density of diapir structures additionally indicates that a mosaic alternation of compression and extension zones (with the latter ones dominant) forms under transpressive conditions.

Comparison of heights of diapir structures above the basement and magnetization of basement rocks (Fig. 8b) shows the presence of two trends with different slopes. The expected regularity is that the heights of structures increase depending on the presence of intensive serpentinization processes, for which the rock volume expands, which pushes blocks, and at the same time, chemical magnetization occurs during the formation of magnetite. Under transpressive conditions, upward pushing increases the heights of structures. Comparison of the heights and thicknesses of the sedimentary cover above the tops of these structures (Figs. 8b, 8c) shows that thicker sediments are observed for small amplitudes of structures (up to 400 ms), whereas for large amplitudes, the structures completely penetrate the cover to reach the surface. Comparison of structures and ages (Fig. 8c) shows a similarity to the distribution of structures with undifferentiated types (Fig. 3): the majority of structures have amplitudes of no more than 400 ms and are grouped into two clusters of 27–38 and 43–53 Ma, corresponding to periods of intensified serpentinization when the upper mantle reached the optimal temperature interval [14]. The values of amplitudes above the mentioned limits are rare, and structures with smaller amplitudes do not pierce the sedimentary cover.

In Fig. 8, two distinct trends with different slopes are the most interesting. The gently sloping trend is the main one and is represented by a large number of structures with the sedimentary cover above their tops; the steep one is characteristic of rare structures without a superimposed cover and with a low magnetization. Such a distribution can be explained by the narrow blocks piercing of the sedimentary cover by some diapir structures with a low degree of serpentinization and low magnetization in zones of weakness (fracture zones), and by their freer growth compared to the main structures of this type.

Stamp Folds

Stamp folds (Fig. 4, profiles 9, 10) in the study area (Fig. 9a) are distributed nearly homogeneously in the sublatitudinal direction, centered on the survey traverses and in blocks between fractures. Morphological interpolation from continuous altimetry-based topography supports the viewpoint that the folds revealed on particular traverses are single folded structures with axes following the configurations of fault troughs. This can be seen from the compilation of seismogeological profiles [8]. The change in sizes of symbols denoting heights of folds above the basement (Fig. 9a) suggests long-period undulation of these heights within the lithospheric block between the Mercury and Vema fracture zones, with a minimum around 50° W and disappearance of folds beyond the limits of the kink-band zone. The zone of low heights coincides with the zone of lower density of diapir structures (Fig. 8a) and negative flower structures (Fig. 6). This argues for the presence of a structural complex related to small local extension orthogonal to the passive parts of fracture zones.

The trend toward an increase in the widths of folds with height is obvious (Fig. 9b). Digitized width and height values increase or decrease with the respective change in another parameter. Within a range up to 17 000 m wide, gentler trends are distinguished, suggesting the advancing growth of fold heights. This is explained by a possible faster vertical increment for narrower units piercing the upper crust. Comparison between widths of folds and Bouguer anomalies (Fig. 9c) shows a fold concentration between 311 and 338 mGal coupled with an increase in their widths in the middle of this range. Note that this range corresponds to certain decompaction of abyssal values of Bouguer anomalies. The background mean values of these anomalies in the abyssal part of the ESA are significantly less (>100 mGal) than in other basins to the north and south (Fig. 9a, inset). Since there also are maximum lateral displacements of segments of the MAR along transform faults with long active parts, we can suggest that deformations, lateral displacements, and the low background of Bouguer anomalies form a group of interrelated geological and geophysical phenomena.

The dependence of the widths of folds on magnetization (Fig. 9d) is demonstrated by a cluster of points beneath the trend: folds in this cluster become narrower as magnetization increases, indicating that more serpentinized blocks containing magnetoactive material have a tendency to form narrow structures that pierce (Fig. 8b) or uplift (Figs. 9b, 9d) the upper crust. This is verified by the formation of serpentinite protrusions substantiated in [2] based on data from the Canary–Bahaman geotraverse.

Imbricate Thrusts

The majority of the region under discussion was studied by submeridional traverses in which imbricate thrusts (Fig. 4, section 3) are nearly absent (Fig. 10a). They were revealed mainly in sublatitudinal passages between traverses and within the limits of the polygon in the eastern part of the studied region. These structures are manifested in the framing of the kink-band zone, also indicating shear movements along the passive parts of fault troughs, because deformations of this type are part of the strike-slip paragenesis [19]. In the survey area with sublatitudinal traverses, thrusts are expressed in all blocks between fractures. Thus, mutual displacements of blocks take place in the entire area with a deformed configuration of the passive parts

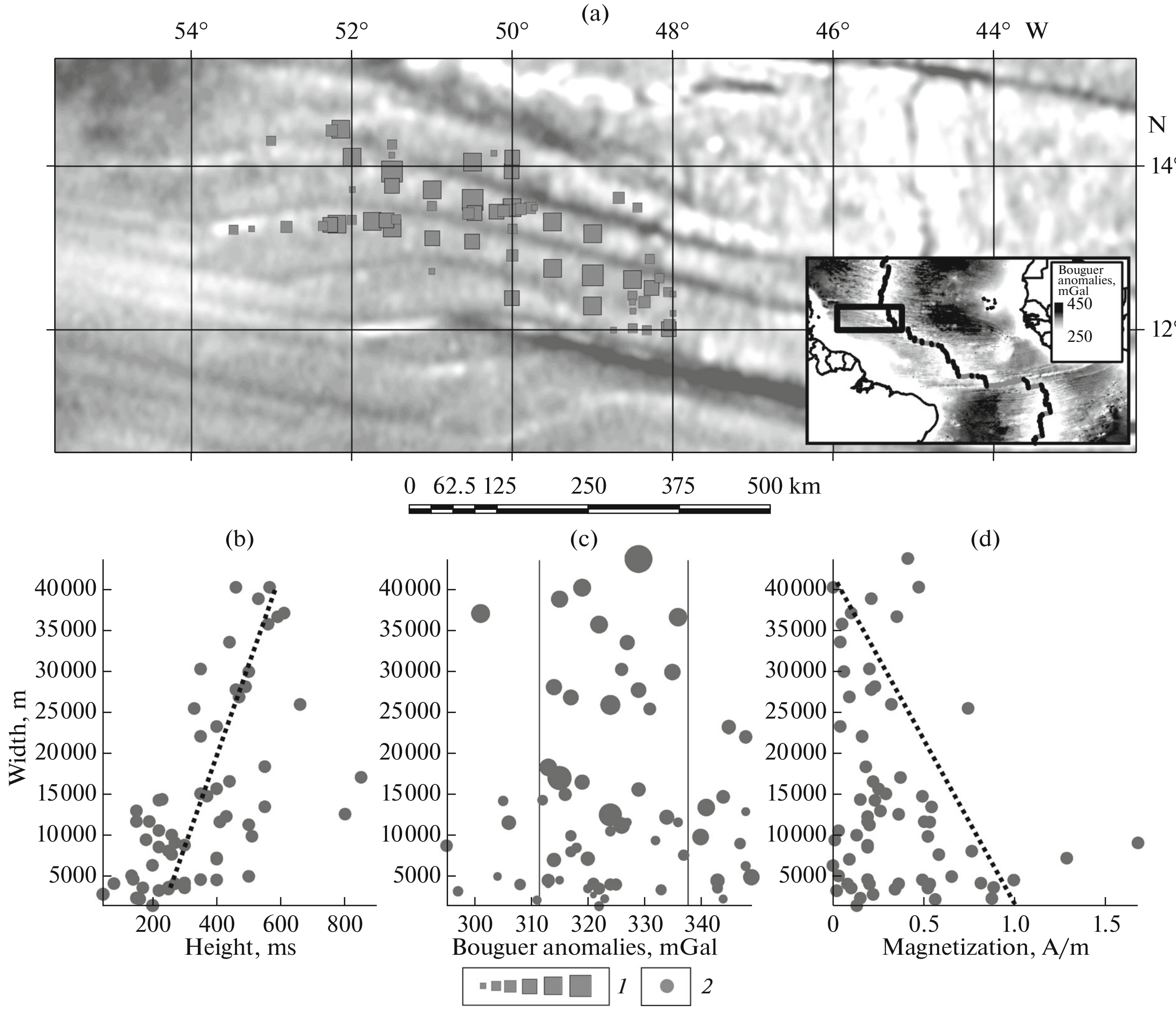

Fig. 9. Stamp folds in ESA west of MAR, based on data from cruise 9 of R/V *Akademik Nikolai Strakhov* (GIN RAS, 1990). (a) General spatial distribution of centers of stamp folds (inset: location of study region in background of normal Bouguer anomalies); (b) correlation between heights and widths of folds (dashed line denotes trend); (c) correlation between widths of folds and Bouguer anomalies (filled circles are proportional to heights of folds graded from 45 to 1020 m; vertical lines delineate interval of Bouguer anomalies with more frequently occurring folds); (d) correlation between widths of folds and magnetization calculated from data on anomalous magnetic field and relief (dashed line denotes trend). Folds: (*1*) graded on height from 45 to 1020 m (in panel (a)); (*2*) in correlation coordinates (in panels (b)–(d)).

of faults. The distribution of vergences, whose directions are oriented as shown by triangles in Fig. 10a, shows that mutual displacement of blocks can be multidirected and makes up a compact group of these forms with different vergences. Most likely, the distribution of vergences occurs due to variations in the directions and values of the displacement vectors for individual blocks between fractures within the general deformation zone. The central part of the region, around 50° W (Fig. 10a), is also anomalous in terms of manifestation of this type of deformations, which are observed along two submeridional traverses, showing the presence of corresponding displacements.

The dependence of the widths of deformations on magnetization (Fig. 10b) shows that the largest objects formed for the minimum values of this parameter. This indicates the absence of its cause-and-effect relationship with serpentinization processes and the influence of shear on their formation. At high values of magnetization, structures with minimum widths form in the framing of narrow serpentinite protrusions. The dependence of deformation amplitudes on the values of Bouguer anomalies (Fig. 10c) is demonstrated by a cluster of them in the range of 310–334 mGal. The analogous range corresponds to the distribution of forced folds (Fig. 9c) on a generally lower background of Bouguer anomalies in the ESA. The distribution of heights of deformations based on basement age (Fig. 10d) shows that recent and present-day deformation processes involve structures of both the

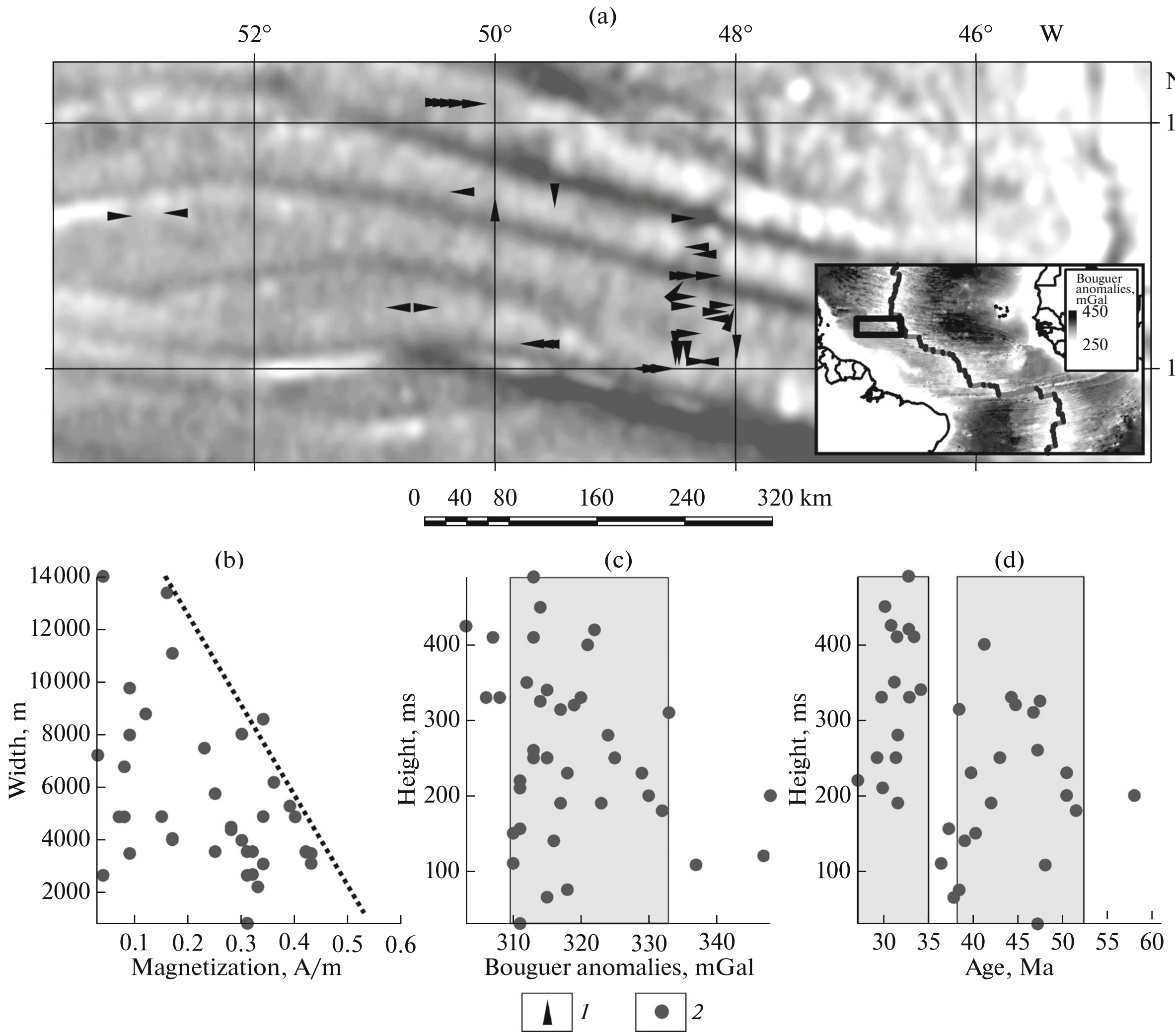

Fig. 10. Imbricate-thrust deformations in ESA west of MAR, based on data from cruise 9 of R/V *Akademik Nikolai Strakhov* (GIN RAS, 1990). (a) General spatial distribution of imbricate-thrust deformations (inset: location of study region on background of normal Bouguer anomalies); (b) correlation between widths of deformations and magnetization calculated from data on anomalous magnetic field and relief (dashed line denotes trend); (c) correlation between heights of deformations and Bouguer anomalies (here and in panel (d), intervals of Bouguer anomalies with more frequently occurring deformations are marked by gray columns); (d) correlation between heights of deformations and age. Thrusts: (*1*) oriented along direction of vergence (in panel (a)); (*2*) not graded, in correlation coordinates (in panels (b)–(d)).

sedimentary cover and basement from all periods of activated serpentinization and the formation of structures with vertical uplift (Fig. 3).

Reverse Faults

The distribution of reverse faults shown in Fig. 11 by symbols proportional to the deformation amplitudes is demonstrated by clear mosaic fragmentation of the stress field, causing formation of faults. Reverse faults are the least represented in the central part of the studied region, around 50° W. Detailed studies within the survey area in eastern part of the region revealed that reverse faults occur more frequently in sublatitudinal traverses, indicating a sublatitudinal orientation of the major tangential stresses that affected the lithosphere in the region and produced faults and deformations in the sedimentary cover. The maximum concentration and amplitude of reverse faults was revealed in the framing of the kink-band zone, in particular, in the northwest, where the azimuths of the passive parts of faults change.

Vertical Acoustic Blanking Anomalies

Vertical acoustic blanking anomalies in seismoacoustic records (gas brightening, also referred to as gas chimneys) are manifestations of fluids in these records: fluids penetrate upwards through weakly consolidated sediments or along fractures. The presence

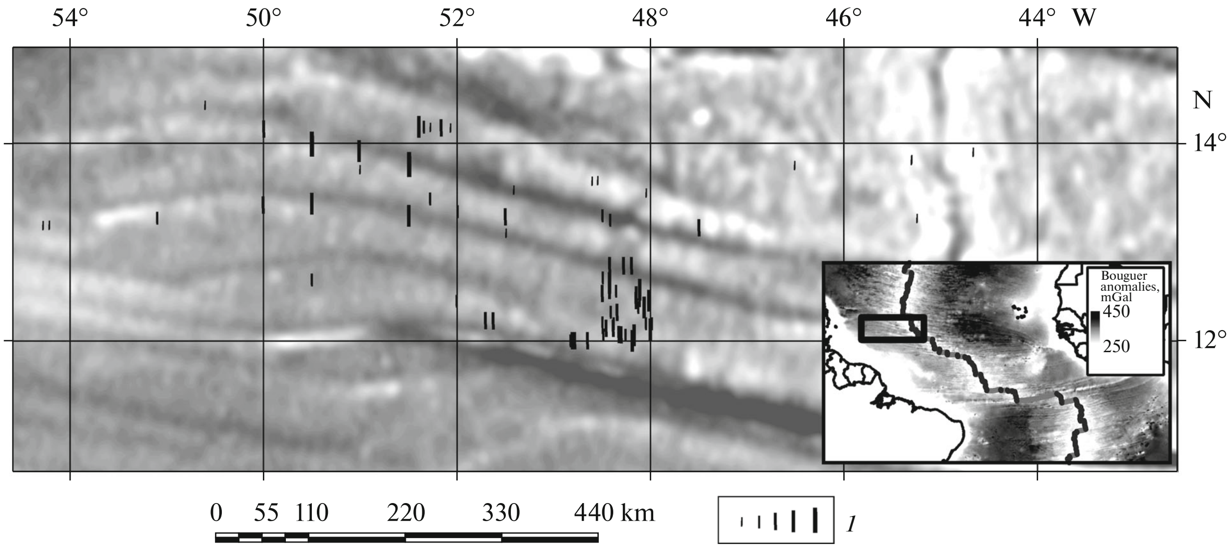

Fig. 11. Reverse faults in ESA west of MAR, based on data from cruise 9 of R/V *Akademik Nikolai Strakhov* (GIN RAS, 1990). Inset: location of study region on background of normal Bouguer anomalies. Vertical lines denoting reverse faults are graded in terms of their amplitudes from 12 to 1100 m.

of this type of record indicates that there are no fluid-impermeable layers along the volume occupied by gas chimneys (Fig. 4, sections 1, 2, 7, 8) and there are no coherent reflectors within this volume. The bases of gas chimneys are in most cases rests on the acoustic basement represented by a basaltic layer, indicating an endogenous source of fluids. Gas chimneys are observed within the entire studied region, but mainly in the axial zones of the passive parts of sediment-filled fault troughs (Fig. 12a). The presence of gas chimneys makes it possible to detect degassing by the CSP method because degassing in water column in the frequency range of CSP (up to ~150 Hz) at depths of a few thousand of meters, with pneumatic seismic sources employed, is nearly unnoticeable. Thus, the finding of gas pipes predominantly in fault troughs does not indicate a total absence of degassing in the bottom parts without sedimentary cover. Nevertheless, the studied region, whose basement ranges from 20 to 60 Ma in age, is nearly completely covered by sediments, except for some rare basement outcrops corresponding to vertical uplifts or piercing of deposits and to reverse-fault dislocations. It follows from this that the abundance of gas pipes in faults is a significant characteristic and an indicator of an endogenous origin of fluids, for which their seepage to the surface is confined to crustal faults. The given depth of transform faults identified in the relief is inferred from the fact that they mainly disappear after calculation of normal Bouguer anomalies (Fig. 12a, inset). A certain number of gas chimneys were revealed around 48° W, in the area of small submeridional displacements, where a detailed area was surveyed.

The dependence of heights of gas chimneys on magnetization (Fig. 12b) indicates a weak and predictable increasing trend, because serpentinization processes lead to both an increase in chemical magnetization and fluid yield [4]. On this background, there are two zones with higher values of heights of gas chimneys, also characterized by a higher fluid yield at the stage of serpentinization development, when the magnetoactive layer with an effective magnetization of about 0.2 and 0.6 A/m was formed, supporting the idea of the presence of certain intervals in which the mentioned processes are activated [14]. Comparison of the heights of gas chimneys and Bouguer anomalies (Fig. 12c) shows that the gas chimneys are clustered within the range of 315–348 mGal, which is lower with respect to the background value in abyssal basins.

Comparison of the heights of gas chimneys and the age of the basement (Fig. 12d) indicates that gas chimneys abruptly began to appear more frequently starting from 37–40 Ma or older. On the younger basement, there is an interval without gas chimneys and a small increase in their abundance on basement younger than 25 Ma. Analysis of the spatial locations of gas chimneys (Fig. 12a) shows that the interval from 25 to 37 Ma where gas chimneys are absent is also expressed in the zone of 49°30′–48°30′ W, where gas chimneys were not revealed. Thus, the majority of gas chimneys coincide with the third interval of deformation concentration (Fig. 3), as obtained without subdivision of deformations into types. The given age distribution can be explained in different ways:

(1) serpentinization processes formed the fluid which was slowly supplied to the sedimentary section;

(2) the fluid was not generated during the first and second (from young to ancient) serpentinization intervals (Figs. 3, 12d), or it was blocked;

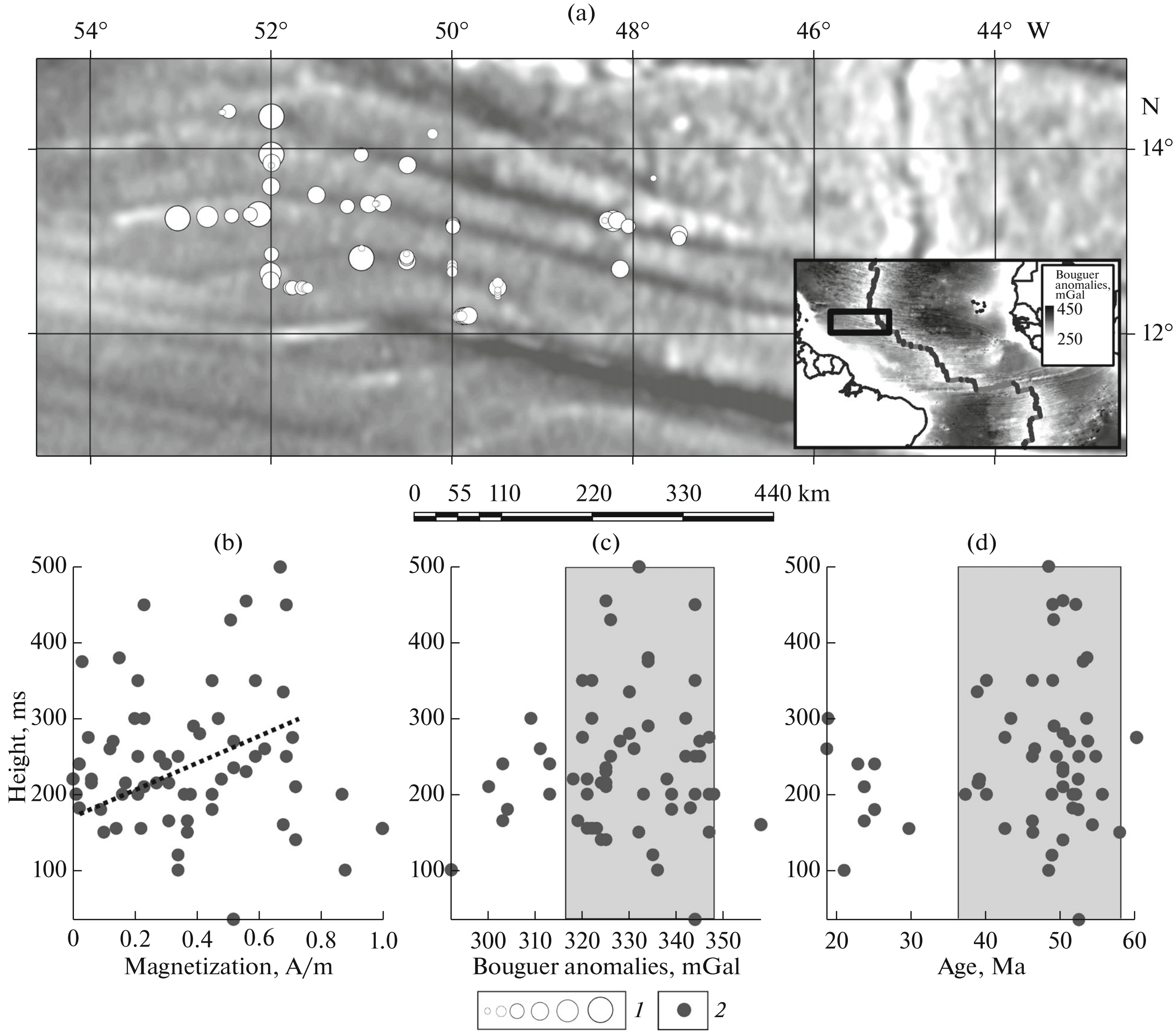

Fig. 12. Vertical acoustic blanking anomalies in seismoacoustic record (gas chimneys) in ESA west of MAR, based on data from cruise 9 of R/V *Akademik Nikolai Strakhov* (GIN RAS, 1990). (a) General spatial distribution of gas chimneys graded in terms of their heights (inset: location of study region on background of normal Bouguer anomalies); (b) correlation between heights of gas chimneys and magnetization calculated from data on anomalous magnetic field and relief (dashed line depicts trend); (c) correlation between heights of gas chimneys and Bouguer anomalies (here and in panel (d), intervals of Bouguer anomalies with more frequently occurring gas chimneys are marked by gray columns); (d) correlation between heights of gas chimneys and age. Gas chimneys: (*1*) graded on height, from 300 to 2670 m (in panel (a)); (*2*) not graded, in correlation coordinates (in panels (b)–(d)).

(3) formation of a kink-band zone that changed configuration of fault zones abruptly increased the possibility of fluid supply into the sedimentary cover, widening fault zones in basement 40 Ma or older in age.

It is difficult to determine exactly which interpretation is correct, but the predominant manifestation of gas chimneys in this area and at the mentioned age of the basement is obvious. Another remarkable feature is that the widths of gas chimneys increase explicitly westward (Fig. 12a), possibly supporting the third interpretation related to widening of fault zones (however, the other two versions are not completely excluded).

Horizontal Acoustic Blanking Anomalies

The horizontal acoustic blanking anomalies in seismoacoustic records within abyssal basins—so-called lenses (Fig. 4, sections 2, 7, 8)—are domains with acoustic stratification that has disappeared, located immediately above the basement. Their distribution in the studied region (Fig. 13a) shows that they are located predominantly in blocks between fractures. If we assume that the source of fluid was the same for both vertical and horizontal acoustic blanking anomalies in seismoacoustic records, then it was supplied ubiquitously. Vertical zones ~240 ms high on average can be found mainly in fault troughs, where the pres-

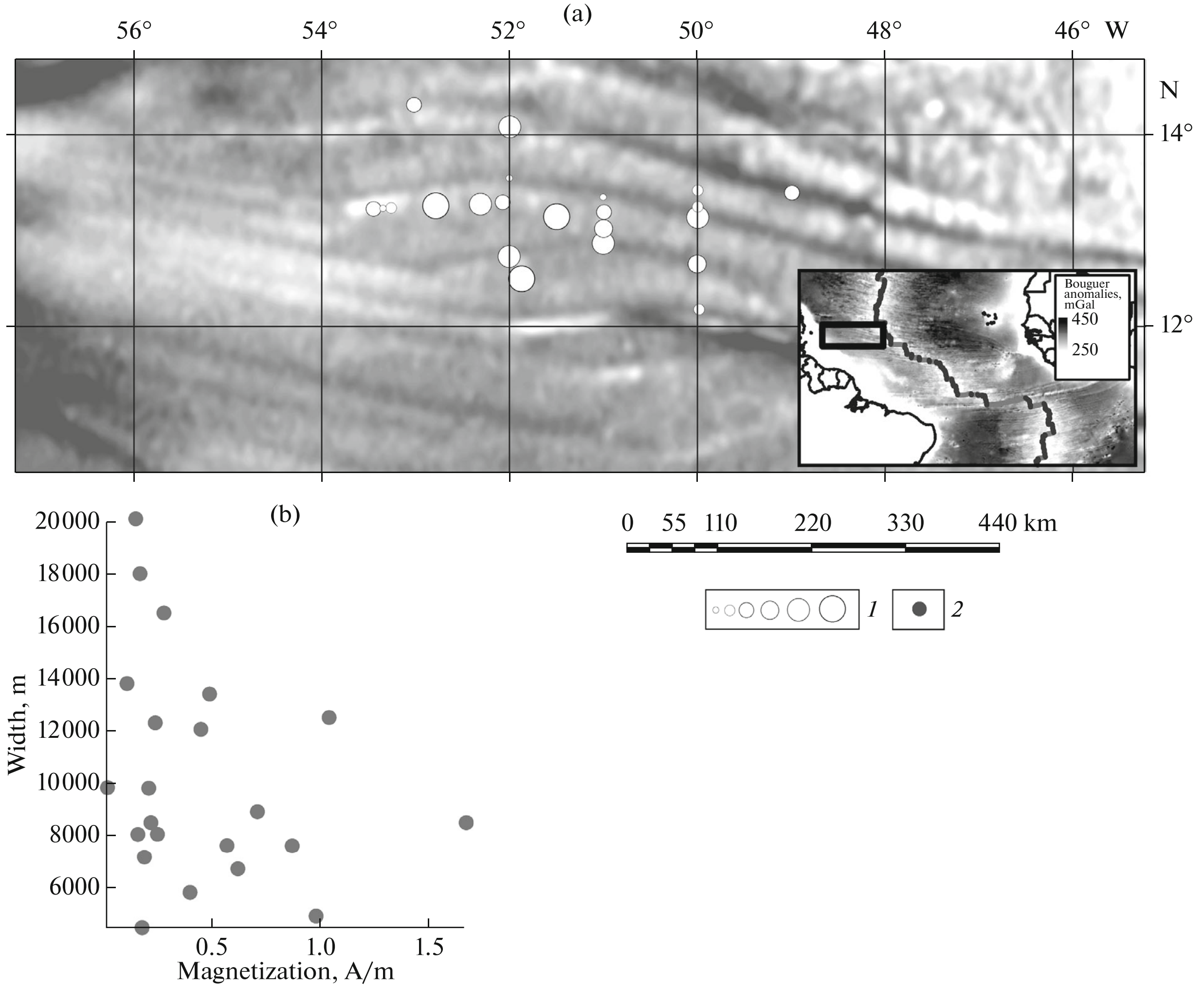

Fig. 13. Horizontal acoustic blanking anomalies in seismoacoustic record (lenses) in ESA west of MAR, based on data from cruise 9 of R/V *Akademik Nikolai Strakhov* (GIN RAS, 1990). (a) General spatial distribution of lenses graded in terms of their widths (inset: location of study region on background of normal Bouguer anomalies); (b) correlation between widths of lenses and magnetization calculated from data on anomalous magnetic field and relief. Lenses: (*1*) graded on width from 4.5 to 20 km (in panel (a)); (*2*) not graded, in correlation coordinates (in panel (b)).

ence of flower structures (Fig. 6) suggests shear displacements leading to fracturing. Horizontal zones ~250 ms thick on average—which is almost the same as the average height of vertical zones—are rarer, and their widths are up to 20 km, whereas vertical zones are ~980 m wide on average. The similarity of vertical extents for vertical and horizontal zones indicates the same fluid progradation rate in sediments, whereas the difference between their widths and structural positions suggests different fracture systems along which endogenous fluid flowed. We can also suggest that there is a fracture system in blocks between faults, but we could not identify it because of sparse submeridional traverses.

Lenses widen westward, and their occurrence on basement 40 Ma or older in age, like for gas chimneys, points to the complete similarity of the processes forming this type of anomalies, except for the geometry of conduits. These channels in the kink-band zone can differ from those in the rest of the studied region, because the distances between fault troughs here are 10–15% larger than those in the remaining part (Fig. 13a). Therefore, small local extensional structures can form, as well as shear and thrust deformations. Comparison of the widths of lenses and magnetization of the basement (Fig. 13b) shows that narrower lenses form for large height values and intensive serpentinization, passing into high vertical zones (Fig. 12b).

GEODYNAMIC SCHEME OF THE EQUATORIAL SEGMENT OF THE WEST ATLANTIC

Analysis of the data on tectonic deformations and fluid anomalies from the CSP record has allowed us to

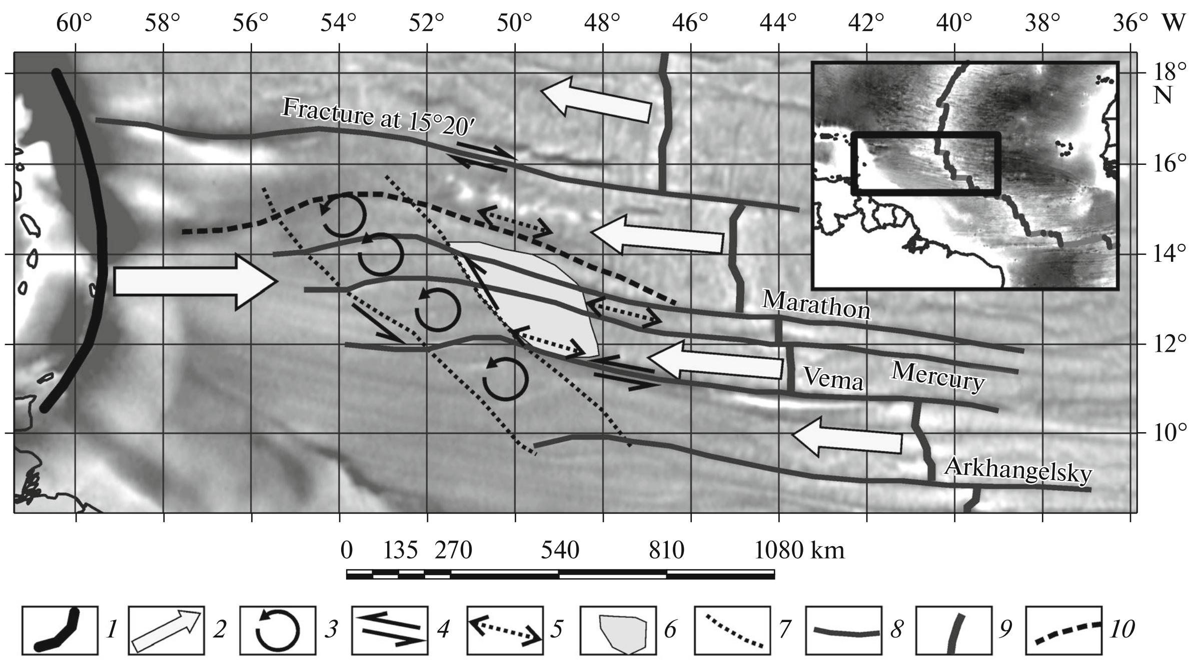

Fig. 14. Geodynamic scheme of ESA of MAR. Inset: location of study region on background of normal Bouguer anomalies: (*1*) Antilles arc; (*2*) direction of Antilles arc effect and movement of plate from MAR; (*3*) counterclockwise rotation of blocks; (*4*) shear displacements; (*5*) alternating shear displacements; (*6*) zone of minimum deformations; (*7*) boundary of kink band; (*8*) transform faults; (*9*) rift axis; (*10*) parallel branch of fault.

compile a geodynamic scheme of the studied region (Fig. 14). The western part of the northern segment of the ESA is located in a zone characterized by negative values of $\delta(Vp/Vs)$ parameter and manifestations of transform faults with large lateral displacement of segments of the MAR. In addition, general decompaction is observed there between the fracture zone at 15°20′ and the Vema Fracture Zone; according to spreading rate data from [25], it is a zone with 10% higher spreading rates compared to the plate segments north and south of it. Since the difference in spreading rates cannot become equal directly beyond the active part of the fracture, shear displacements in passive parts continue to exist at distances comparable to the lengths of active parts. This process causes the plate to be partitioned into particular blocks along passive parts of faults with the formation of tectonic breccias and serpentinites [8]; note that plate fragments can be activated along zones of weakness with variations in their motion parameters. In this respect, dextral and sinistral strike slips are indicated along passive parts of the fracture zone at 15°20′ and the Vema Fracture Zone. According to the data from [22], foundation of the Antilles arc is dated back to as early as ~10 Ma ago. Its effect on the northern segment of ESA (Fig. 14) led to the formation of kink-band zone that changes configuration of passive parts of transform faults—remarkably, only in the latitude interval of the arc extent. Additionally, this effect led to reorientation of the Vema Fracture Zone's fault trough [20] to the position orthogonal to the Antilles arc. Formation of this arc was most likely caused by penetration of a branch of the plume that formed the East Pacific Rise along the Galapagos Rift into the Atlantic from the west, as seen from seismic tomography imaging [23].

Formation of the kink-band zone is associated with displacements of lithospheric blocks with counterclockwise rotation. This leads to deformations related to compression and vertical uplift of crustal blocks and to the formation of local extension zones favoring degassing of endogenous fluid. The sublatitudinal orientation of imbricate thrusts with various vergences points to inhomogeneity of shear displacements with the lateral effect on blocks between fractures: in the scheme (Fig 14), this is indicated by the alternating displacements along transform faults. The superposition of the general vector of plate motion from the MAR with respect to the effect of the Antilles arc forms the area to the east of the kink-band zone. Here, deformations are the least expressed and their maximum amplitudes are observed in the periphery of this area and in the kink-band zone itself. In the north, this area is bounded by the fault trough of a parallel branch of the Marathon Fault, along which shear displacements of alternating directions are also possible. The kink-band zone also formed along the primary inhomogeneous structure of the plate that emerged due to an abrupt change in the parameters of plate motion 70 to 50 Ma ago, as well as to the westward shift of the Eulerian pole. This led to a change in the spreading direction, bends of transform faults along the entire North Atlantic, and formation of a rift in the Labrador Sea. This is the basement age interval (70 to 50 Ma), with the initially formed inhomogeneity, in which the kink-band zone formed under the influence of the Antilles arc.

SYNTHESIS OF THE RESULTS

The features of fluids in seismoacoustic records are (a) the loss of acoustic stratification and chaotization of layers, (b) contrasting gas caps, (c) subsidence of synphase axes, (d) narrow vertical acoustic blanking anomalies (related to fluid penetration) in seismoacoustic records, (e) acoustic blanking anomalies within sediments adjacent to the basement in seismoacoustic records, and (f) the occurrence of anomalies in the instantaneous frequency attribute.

The features of fluid penetration into water from the sedimentary cover that accumulates mobile components are (a) characteristic wave diffraction with peaks above the surface of the bottom, (b) loss of acoustic stratification, (c) a brightened and chaotic pattern of the record in the upper part of the section beneath the penetration zone, (d) local bulging of the bottom, and (e) formation of either sedimentary-material fans or pockmarks.

Fluid anomalies are encountered above diapir structures, fault zones, and probably in areas with a degraded gas hydrate layer acting as fluid seal, in addition to lithologically low-permeable sediments.

Manifestations of fluids spatially coincide with sublatitudinal zones of MAR-induced activated deformations within basins with depths of 1700 m greater, as well as the zones with negative density anomalies, such as Hess-type crust around the fracture at 15°20′ and in the South Atlantic at 20°–24° S. Deformation zones are represented by a variety of strike-slip displacements in combination with compression and extension. The decrease in density during serpentinization forms gravity anomalies that exceed the accuracy of altimetry data and makes it possible to spot these zones from remote sensing data.

A considerable number of deformation structures are units related to vertical uplift of the sedimentary basement in narrow and wide blocks, degassing-related ascent, and transpressive flow of both recent and present-day age. Spatially, they tend to be near NW-oriented kink bands crossing the northern segment of the ESA. The height histogram for structures undifferentiated by type has a main peak at about 400 m. During serpentinization, the origin of vertical pressing out of basement blocks, the thickness of the layer involved in serpentinization is up to 2 km. The polymodality of distribution indicates repeated activation of processes in the vicinity of these structures. There is a descending dependence of the depth of the bottom near these structures on the age of the basement: it appears linear, with a step of about 20 Ma and a more gently sloping gradient after this age. The main trend in the heights of structures has a form gently sloping upward from 400 to 600 m in the interval of 0–20 Ma and then with an even gentler ascent to 700 m with three overlapping zones with abruptly higher values at 6–16 Ma (Middle–Late Miocene), 27–38 Ma (Oligocene), and 43–53 Ma (Early–Middle Eocene).

Such a distribution can occur due to the magnetic properties of serpentinites, which vary as a function of decreasing temperature of the upper mantle combined with local activation of diapiric processes after a certain temperature is reached. The age of the basement does not correspond to the age of structures but may reflect the evolution of temperature. In the intervals between zones with high structures, there are break points of the relief, which are related to phase transitions at the base of the lithosphere.

Deformation structures based on 2D CSP data were categorized in the direction of mass displacements in the vertical plane of the section. The following types of tectonic structures were distinguished:

(1) imbricate-thrust deformations expressed as bulging under horizontal displacement;

(2) diapir (piercement) structures related to positive vertical displacements;

(3) stamp folds related to wide basement blocks;

(4) deformations related to the ascent of fluids.

Deformations related to vertical movements are typical of the flanks of the MAR, where cooling of the lithosphere is maximum. In these areas, the sedimentary cover is usually thin; therefore, these deformations can hardly be identified from deformations of the cover. Negative displacements also take place during transtension in the passive parts of faults. Sediment bedding anomalies related to contour currents and turbidite flows (which do not have a tectonic nature) have also been distinguished. In the studied basin, there are areas where the seismofacies of these flows are not observed. The most frequently encountered deformations of the sedimentary cover within the studied region are (a) vertical acoustic blanking anomalies in seismoacoustic records (gas chimneys), (b) stamp folds and diapir structures, (c) reverse faults, (d) imbricate-thrust systems, and (e) horizontal acoustic blanking anomalies in seismoacoustic records.

In particular, types of deformation related to strike slips should be mentioned: negative and positive flower structures revealed in the passive parts of transform faults. Data on differences in the spreading rates for different parts along the MAR allow us to conclude that slipping is possible in the passive parts of transform faults.

The general spatial distribution of deformational and other types of anomalous patterns in the seismoacoustic record demonstrates their maximum concentration in zones with a higher degree of macrofracturing above cold blocks revealed from analysis of the tomographic $\delta(Vp/Vs)$ attribute and confirms the first two elements in the sequence of intraplate phenomena: the contrasting geodynamic state of the mantle and macrofracturing. The occurrence frequency of folded units decreases closer to the MAR due to the small values of the sediment thickness.

Detection of structures pertaining to strike-slip paragenesis in the sedimentary cover above the passive parts of transform faults indicates the existence of shear displacements between segments of the oceanic lithosphere after their spreading-induced removal beyond the limits of active parts. Positive flower structures formed in a transpressive regime are located at the bends of the Marathon and Mercury fractures framing the structural kink band in the north. Within this framing, rare manifestations of negative flower structures indicate a local extensional component in the mosaic of stresses.

The studied region is framed in the south by the western passive part of the Vema Fracture Zone, where the median ridge (indicator of shearing with compression) is identified in the field derived from altimetry and CSP data. Thus, transpressive conditions are observed in most passive parts of faults framing the kink-band zone.

The spatial distribution of the most frequently revealed deformations in the northern segment of the ESA to west of the MAR shows a higher concentration of deformations with a positive vertical motion component, framed by a kink band that changes the normal configuration of the passive parts of transform faults. A similar distribution is observed for positive flower structures in fault troughs and for diapir structures, stamp folds, thrust-related deformations, and reverse faults. This produces a mosaic distribution with a clear minimum of the number and amplitude of these structures in the central part of the studied area, between 50°30′ and 48°30′ W, which supports the probable character of the stress distribution. A specific feature of the distribution of reverse-fault and thrust deformations is their sublatitudinal vergence with alternating direction. Joint analysis of the magnetization and heights of diapir structures shows a direct relationship between these heights, on the one hand, and the intensity of magnetization and development of serpentinization processes, on the other. The width of stamp folds demonstrates an inverse dependence on magnetization, which is a tendency toward protrusion under conditions of narrow serpentinization zones. The absence of a relationship between magnetization and reverse-fault/thrust deformations suggests their predominantly shear origin. Deformations are present in the Bouguer anomaly range of ~310–340 mGal, which is considerably lower than the background value in the adjacent abyssal basins. This indicates that deformations are related to decompaction and how decompaction occurs in the vicinity of faults with large lateral displacement of the MAR axis. In terms of basement age, deformations are clustered within two time intervals, 27–38 and 43–53 Ma; the basement corresponding to these intervals lies under a thick sedimentary cover, which makes it possible to identify deformations from characteristic patterns of the seismoacoustic record.

The distribution of fluid-related anomalies shows their ubiquitous presence within the Bouguer anomaly range of ~310–340 mGal, but gas chimneys are manifested predominantly along fault troughs, whereas lenses can mostly be found within blocks between fractures. Note that all types of anomalies adjoin the acoustic basement: this suggests their endogenous origin. Widths of anomalies regularly grow westwards as serpentinization processes become older. The anomalies in the seismoacoustic record related to the loss of acoustic stratification owing to fluid penetration were formed by one source, but they removed from the basement into weakly consolidated sediments through different fracture systems. Gas chimneys and lenses are of almost the same height and thickness within sediments, and they are characterized by the same rates of fluid penetration upsection. Their comparison with magnetization has revealed regular growth in fluid-related anomalies with amplitudes, surging within two magnetization intervals. We emphasize that fluid-related anomalies are almost completely absent above basement younger than 40 Ma, the zone of which corresponds to one with tectonic deformations moderate in amplitude. This takes place either owing to the specific character of fluid penetration from the basement into sediments, which causes a delay in the formation of fluid-related anomalies, or due to stresses in the lithosphere: under these stresses, sites of local extension form in the framing zone of kink bands, promoting fluid release.

CONCLUSIONS

(1) When compared with geophysical fields, intraplate deformations in the ESA and degassing zones in the sedimentary cover, which are identified from aggregate features in seismic profiling records and associated with the inhomogeneous state of the upper mantle and macrofracturing, indicate the presence of vertical displacements of basement blocks due to decompaction and additional magnetization of rocks in the upper part of the crystalline layer, which occurred from serpentinization of rocks in the upper mantle.

(2) Analysis of seismic sections from area and traverse surveys shows the presence of shear deformations in combination with compression and extension beyond the limits of the MAR (flower structures, imbricate thrusts, and median ridges) and deformations characterized by vertical uplift of basement blocks with an amplitude of 400 m on average (diapir structures, reverse faults, stamp folds, and acoustic

blanking anomalies in seismoacoustic records, recognized as lenses and gas chimneys).

(3) Intraplate deformation phenomena, combined with analysis of geophysical fields, form the following unambiguous cause-and-effect sequence of phenomena and processes: a contrasting lateral geodynamic state of the mantle; inhomogeneous horizontal displacements that formed over time as the lithosphere cooled, such as macrofracture features tectonic like strike slips and associated deformations, and isostatic compensation of local vertical displacements; penetration of water into the upper mantle through faults and fractures; establishment of conditions favorable for serpentinization of rocks in the upper mantle, accompanied by formation of decompaction zones, and local negative-gravity and higher-magnetization anomalies; the appearance of deformations related to vertical uplift of the basement and sedimentary cover blocks, accompanied by the generation of fluids (chiefly methane); accumulation of fluids in the sedimentary cover and their penetration into water, associated with the formation of anomalies in seismoacoustic records.

ACKNOWLEDGMENTS

The study was supported by the Russian Foundation for Basic Research (project no. 15-05-05888; S.Yu. Sokolov). The seismoacoustic record elements related to the formation of submarine landslides and other geological hazards were digitized in part under state contract no. 0135-2016-0013 for the Geological Institute of the Russian Academy of Sciences (A.O. Mazarovich). Manifestations of degassing in the sedimentary cover in seismoacoustic records were digitized partially under state contract no. 0135-2015-0022 and supported by the Presidium of the Russian Academy of Sciences (Program no. 3).

REFERENCES

1. M. P. Antipov, V. V. Eremeev, and S. M. Zharkov, "Structure of the sedimentary cover in the central sector of the Atlantic in the region of Cape Verde," in *Structure of the Sedimentary Cover in the Central Atlantic*, Vol. 449 of *Tr. Geol. Inst. Ross. Akad. Nauk* (Nauka, Moscow, 1990), pp. 95–110.
2. E. G. Astafurova, A. M. Gorodnitskii, S. V. Luk'yanov, and S. P. Mashchenkov, "Nature of magnetic anomalies and structure of the oceanic crust of the Mid-Atlantic Ridge and adjacent basins along the Canaries–Bahamas geotraverse," in *Nature of Magnetic Anomalies and Structure of Oceanic Crust*, Ed. by A. M. Gorodnitskii (Vseross. Nauchno-Issled. Inst. Rybn. Khoz. Okeanogr., Moscow, 1996), pp. 171–202.
3. *Deep Structure and Evolution of Lithosphere in the Central Atlantic: Study Results for the Canaries–Bahamas Geotraverse*, Ed. by S. P. Mashchenkov and Yu. E. Pogrebitskii (VNIIOkeangeologiya, St. Petersburg, 1998) [in Russian].
4. L. V. Dmitriev, B. A. Bazylev, S. A. Silant'ev, M. V. Borisov, S. Yu. Sokolov, and A. Bugo, "Hydrogen and methane formation when serpentinization of mantle hyperbasites in oceans with respect to petroleum origination," Ross. Zh. Nauk Zemle **1**, 511–519 (1999).
5. O. V. Levchenko, L. R. Merklin, and N. N. Sviridov, "Structure of sedimentary cover and basement relief of deep basins of the Atlantic and Indian oceans," in *Geophysical Fields and Seafloor Structure in Oceanic Basins*, Ed. by Yu. P. Neprochnov (Nauka, Moscow, 1990), pp. 89–119.
6. V. L. Lomtev, "Structure and evolution of abyssal mounds in the Northwestern Plate of the Pacific from the continuous seismic profiling and seismic stratigraphy data," Geodin. Tektonofiz. **7**, 273–288 (2016). doi 10.5800/GT-2016-7-2-0206
7. A. O. Mazarovich and S. Yu. Sokolov, "Recent deformations of the sedimentary cover in passive parts of the Arkhangel'sky, Doldrums, and Vernadsky fracture zones, Atlantic Ocean," Dokl. Earth Sci. **357**, 1320–1323 (1997).
8. A. O. Mazarovich, *Geological Structure of the Central Atlantic: Faults, Volcanic Edifices, and Ocean Floor Deformations* (Nauchnyi Mir, Moscow, 2000) [in Russian].
9. A. O. Mazarovich and S. Yu. Sokolov, "Anisotropy of intraplate deformations of the Atlantic Ocean," in *Contemporary Problems of Geology*, Vol. 565 of *Tr. Geol. Inst. Ross. Akad. Nauk* (Nauka, Moscow, 2004), pp. 221–250.
10. C. P. Mashchenkov, E. M. Litvinov, A. G. Gorshkov, and I. P. Lukashevich, "Geophysical criteria of distinguishing the regional settings favorable for deep polymetallic sulfides to form," in *Deep Structure and Geodynamics of Lithosphere of the Atlantic and Pacific Oceans*, Ed. by I. S. Gramberg and P. A. Stroev (Nauka, Moscow, 1992), pp. 151–178.
11. V. A. Panaev and S. N. Mitulov, *Seismostratigraphy of Sedimentary Cover of the Atlantic Ocean* (Nedra, Moscow, 1993) [in Russian].
12. A. I. Pilipenko, "Tectonic deformations of the Brazil Basin," Dokl Akad. Nauk **330**, 484–487 (1993).
13. A. I. Pilipenko, "Tectonic compression structures in the western flank of the Mid-Atlantic Ridge, 8°–12° S," Dokl Akad. Nauk **340**, 664–666 (1995).
14. K. V. Popov, B. A. Bazylev, and V. P. Shcherbakov, "Temperature range for magnetization of oceanic spinel peridotites," Oceanology **46**, 256–267 (2006).
15. E. I. Pristavakina, Candidate's Dissertation in Physics and Mathematics (Moscow, 1984).
16. S. Yu. Sokolov, "Tectonic peculiarities of the Mid-Atlantic Ridge from the correlation between surface parameters and geodynamic state of the upper mantle," Vestn. KRAUNTs. Nauki Zemle, No. 4, 88–105 (2016).
17. S. Yu. Sokolov, "Sedimentary cover deformation in the equatorial Atlantic and their comparison with geophysical fields," Geotectonics **51**, 74–88 (2017).

18. O. G. Sorokhtin and S. A. Ushakov, *Nature of Tectonic Activity of the Earth*, Vol. 12 of *Itogi Nauki Tekh., Ser.: Fiz. Zemli* (VINITI, Moscow, 1993) [in Russian].
19. A. I. Timurziev, Doctoral Dissertation in Geology and Mineralogy (Moscow, 2009).
20. E. Bonatti, D. Brunelli, W. R. Buck, A. Cipriani, P. Fabretti, V. Ferrante, L. Gasperini, and M. Ligi, "Flexural uplift of a lithospheric slab near the Vema transform (Central Atlantic): Timing and mechanisms," Earth Planet. Sci. Lett. **240**, 642–655 (2005).
21. K. O. Emery and E. Uchupi, *The Geology of the Atlantic Ocean* (Springer, New York, 1984).
22. K. D. Klitgord and H. Schouten, "Plate kinematics of the central Atlantic," in *Geology of North America*, Ed. by P. R. Vogt and B. E. Tucholke (Geol. Soc. Am., Boulder, Color., 1986), pp. 351–378.
23. C. Li, R. D. van der Hilst, E. R. Engdahl, and S. Burdick, "A new global model for *P* wave speed variations in Earth's mantle," Geochem., Geophys., Geosyst. **9** (2008). doi 10.1029/2007GC001806
24. S. Maus, U. Barckhausen, H. Berkenbosch, N. Bournas, J. Brozena, V. Childers, F. Dostaler, J. D. Fairhead, C. Finn, R. R. B. von Frese, C. Gaina, S. Golynsky, R. Kucks, H. Luhr, *P.* Milligan, et al., "EMAG2: A 2-arc-minute resolution Earth Magnetic Anomaly Grid compiled from satellite, airborne and marine magnetic measurements," Geochem., Geophys., Geosyst. **10** (2009).
25. R. D. Muller, M. Sdrolias, C. Gaina, and W. R. Roest, "Age, spreading rates, and spreading asymmetry of the world's ocean crust," Geochem., Geophys., Geosyst. **9** (2008).
26. D. T. Sandwell and W. H. F. Smith, "Global marine gravity from retracked Geosat and ERS-1 altimetry: Ridge segmentation versus spreading rate," J. Geophys. Res.: Solid Earth **114** (2009). doi 10.1029/2008JB006008
27. GEBCO 30" Bathymetry Grid, version 20141103, 2014. http://www.gebco.net. Accessed December 15, 2014.

Reviewers: E.P. Dubinin, T.N. Kheraskova

Translated by N. Astafiev